
Visual Attention Drifts, but Anchors Hold: Mitigating Hallucination in Multimodal Large Language Models via Cross-Layer Visual Anchors

Chengxu Yang¹ Jingling Yuan¹ Chuang Hu² Jiawei Jiang²

Abstract

Multimodal Large Language Models often suffer from object hallucination. While existing research utilizes attention enhancement and visual retracing, we find these works lack sufficient interpretability regarding attention drift in final model stages. In this paper, we investigate the layer wise evolution of visual features and discover that hallucination stems from deep layer attention regressing toward initial visual noise from early layers. We observe that output reliability depends on acquiring visual anchors at intermediate layers rather than final layers. Based on these insights, we propose CLVA, which stands for Cross-Layer Visual Anchors, a training free method that reinforces critical mid layer features while suppressing regressive noise. This approach effectively pulls deep layer attention back to correct visual regions by utilizing essential anchors captured from attention dynamics. We evaluate our method across diverse architectures and benchmarks, demonstrating outstanding performance without significant increase in computational time and GPU memory.

1. Introduction

The rapid development of Multimodal Large Language Models (MLLMs) has revolutionized artificial intelligence by enabling seamless integration of visual and textual information(Chen et al., 2023; Dai et al., 2023). These models demonstrate impressive performance across various tasks, including Visual Question Answering (VQA), image captioning, and multimodal reasoning(Chen et al., 2024). However, MLLMs are often hindered by hallucination issues, where generated outputs deviate from or fabricate details inconsistent with the provided visual content(Huang et al.,

2024; Park et al., 2025). This problem significantly undermines the models’ reliability and trustworthiness in practical applications.

Numerous research efforts are dedicated to mitigating hallucinations in MLLMs without retraining; these methods fall into three main categories: (i) contrastive decoding techniques(Wan et al., 2025; Wang et al., 2025) compare outputs from different decoding paths to suppress hallucinations, yet they double the inference cost; (ii) attention modification approaches(Yin et al., 2025; Chen et al., 2025) enhance the model’s focus on visual content by altering attention weights, but they risk amplifying hallucinatory elements; and (iii) layer injection strategies(Zou et al., 2024; Wang et al., 2024a) propagate early-layer representations to later layers for better grounding, although their interpretability remains underexplored.

Prior studies have observed that factual tokens in MLLM outputs tend to decrease in later layers while hallucinatory tokens increase(Li et al., 2025c). Consequently, existing approaches mitigate this issue by weighting later-layer logits based on early-layer logits or employing Visual Retracing to allow models to reuse decoded content from earlier stages. However, the underlying reasons for the decline in factual content accuracy in later layers remain unexplored. Some works suggest that MLLMs possess implicit knowledge of where to attend in images(Zhang et al., 2025; Li et al., 2025b). In this work, we visualize multi-head attention to visual content through heatmaps and conduct detailed analyses of attention scores. Our findings provide deeper insight into this phenomenon on two fronts: first, visually sensitive heads demonstrate precise and concentrated focus on query-relevant regions in mid-layers; second, this focus diverges in later layers, scattering toward regions remarkably similar to those attended in early layers by visually insensitive heads.

Building on this discovery, we propose the Cross-Layer Visual Anchors (CLVA), a training-free plug-and-play approach designed to enhance visual grounding in MLLMs. During the forward pass, CLVA first distinguishes visually sensitive heads from visually insensitive heads based on their attention to image tokens. It then extracts robust visual anchor patterns: concentrated regions from mid-layer visually sensitive heads and divergent noisy regions from

¹School of Computer Science and Artificial Intelligence, Wuhan University of Technology, China ²School of Computer Science, Wuhan University, China. Correspondence to: Chengxu Yang <311368@whut.edu.cn>.

early-layer visually insensitive heads. In later layers, CLVA adaptively refines text-to-image attention by amplifying focus on the concentrated anchor regions while suppressing attention to the divergent ones. This selective refinement effectively counters the observed attention divergence, providing a clear mechanistic explanation for the factual content degradation in deeper layers. Empirical evaluations across multiple hallucination benchmarks confirm the effectiveness of CLVA, yielding consistent improvements in factual accuracy. At the same time, the module introduces minimal computational overhead and preserves near-original inference speed.

In summary, our key contributions are as follows:

- We explore the progressive decline in factual grounding within MLLMs. Multi-head attention heatmaps and attention score analyses reveal that attention in later layers collapses toward the distribution patterns of early insensitive heads.
- We propose the CLVA. This module employs a visual anchor mechanism to extract robust patterns from early visually insensitive heads and mid-layer visually sensitive heads for targeted refinement in later layers.
- We develop CLVA as a training-free solution. The design supports plug-and-play integration, avoids multi-pass decoding, ensures broad compatibility across models, and adds negligible computational overhead.
- We perform comprehensive evaluations on hallucination benchmarks. Results confirm gains in factual accuracy and visual grounding.

2. Related Work

2.1. Multimodal Large Language Models

Multimodal Large Language Models (MLLMs) integrate visual perception and language understanding by connecting a pre-trained vision encoder to a large-scale language decoder (Devlin et al., 2019; Li et al., 2022). Early models such as BLIP-2 (Dai et al., 2023) and miniGPT-4 (Zhu et al., 2024) introduced intermediate modules like the Q-Former (Wadkar et al., 2024) to bridge modalities effectively. More streamlined approaches, exemplified by LLaVA (Liu et al., 2024a), use simple linear mappings to align visual tokens directly into the language space, reducing complexity while maintaining strong results. Recent models, including LLaVA-Next (Liu et al., 2024b) and GLM4V (Wang et al., 2024b), adopt a two-stage training process: initial pre-training for modality alignment followed by instruction tuning to refine prompt-following behavior. Despite these innovations, hallucinations persist as a core

limitation, where generated text misaligns with visual inputs by fabricating unsupported details.

2.2. Hallucination Mitigation in MLLMs

Hallucination in language models originated in unimodal LLMs, where it describes generated content that deviates from factual knowledge or user instructions (Huang et al., 2025; Yang et al., 2025; Bai et al., 2024). MLLMs inherit this problem and extend it to the visual domain, producing text that misaligns with or fabricates details absent from the input image (Jiang et al., 2025; Cho et al., 2025). Numerous mitigation strategies require additional training. These include curating more robust instruction datasets, applying reinforcement learning with human or AI feedback, and enhancing model architectures (Zhu et al., 2025; Yu et al., 2025). Although such methods yield notable improvements, they demand extensive data preparation and costly fine-tuning.

Training-free approaches provide a resource-efficient alternative by intervening only at inference time. Contrastive decoding methods, such as VCD (Leng et al., 2024a), ICD (Wang et al., 2024c), and IMCCD (Li et al., 2025a), generate parallel output distributions from original and perturbed inputs to favor factual content, though they typically double inference cost due to multiple forward passes. ClearSight (Yin et al., 2025) amplifies visual signals in middle-layer fusion to overcome insufficient visual attention. VisFlow (Tang et al., 2025) modulates attention dynamics at token and head levels to emphasize salient visual regions while suppressing linguistic bias. MemVR (Zou et al., 2024) introduces a look-back mechanism that conditionally re-injects visual tokens as key-value memory upon detecting high uncertainty. DeCo (Wang et al., 2024a) dynamically corrects later-layer logits by incorporating knowledge from preceding layers. These approaches commonly exploit the stronger visual attention observed in mid-layers to counteract degradation in deeper layers. However, they offer limited insight into internal model dynamics and fail to investigate why factual accuracy declines progressively across layers, particularly the role of cross-layer attention divergence. CLVA bridges this gap with an explicit mechanistic explanation and targeted refinement grounded in patterns from visually sensitive and visually insensitive heads.

3. Motivation

3.1. Functional Diversity across Attention Heads

Our investigation begins with an empirical analysis of the cross-modal attention mechanisms within the LLaVA1.5-7B (Liu et al., 2024a), which consists of $L = 32$ Transformer layers, each containing $H = 32$ attention heads. We aim to quantify the degree to which different heads allocate

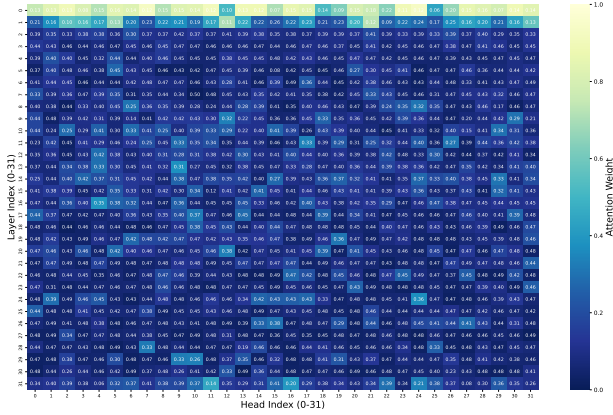


Figure 1. Matrix visualization of visual attention intensity across 32 layers and 32 heads in LLaVA. Colors represent the average attention weights to visual tokens T_{vis} , while numbers denote the average attention weights to system and text prompt tokens.

focus toward visual information during the autoregressive decoding process. Following the VisFlow (Tang et al., 2025), for each layer $l \in \{1, \dots, L\}$ and head $h \in \{1, \dots, H\}$, we compute the visual attention intensity $\Phi_h^{(l)}$ as the mean attention weight assigned from the set of text tokens T_{txt} to the visual token sequence T_{vis} :

$$\Phi_h^{(l)} = \frac{1}{|T_{txt}|} \sum_{i \in T_{txt}} \sum_{j \in T_{vis}} \mathbf{A}_h^{(l)}(i, j) \quad (1)$$

where $\mathbf{A}_h^{(l)}$ denotes the cross-modal attention sub-matrix of the h -th head at layer l .

As illustrated in Figure 1, we visualize the scores calculated by Eq. 1 in a 32×32 intensity matrix, where each cell (l, h) represents the average grounding strength of a specific head at a given layer. The visualization reveals a distinct sparsity pattern: visual grounding is not a distributed property across the entire architecture but is instead concentrated within a specialized subset of heads, and this pattern varies across layers. Based on this observation, we categorize the heads into visually sensitive heads (\mathcal{H}_{sens}) and visually insensitive heads (\mathcal{H}_{insens}) through a distribution-based thresholding mechanism:

$$\mathcal{H}_{sens}^{(l)} = \{h \in H \mid \Phi_h^{(l)} > \mu_{\Phi}^{(l)} + \lambda_{vis} \sigma_{\Phi}^{(l)}\} \quad (2)$$

$$\mathcal{H}_{insens}^{(l)} = \{h \in H \mid \Phi_h^{(l)} < \mu_{\Phi}^{(l)} - \lambda_{vis} \sigma_{\Phi}^{(l)}\} \quad (3)$$

where $\mu_{\Phi}^{(l)}$ and $\sigma_{\Phi}^{(l)}$ denote the mean and standard deviation of visual attention intensity within layer l , respectively. The λ_{vis} is a hyperparameter that adjusts the selection threshold for functional heads, which we set to 1 in our experiments. This formalization provides a principled basis for isolating

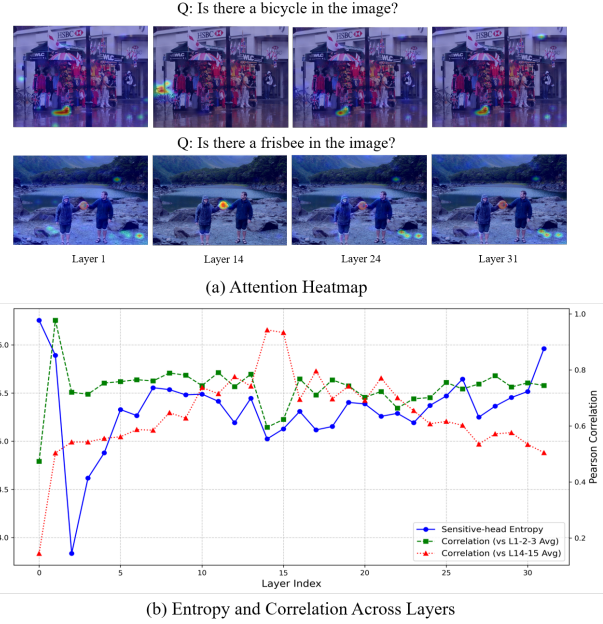


Figure 2. Attention analysis on LLaVA-1.5-7B. (a) Heatmap visualization of attention patterns across different layers. (b) Statistical metrics where the blue line represents the average attention entropy of vision sensitive heads. The green and red lines denote the Pearson correlation coefficients between the attention distributions of each layer and the mean attention of insensitive heads in initial layers and sensitive heads in intermediate layers, respectively.

functional heads that drive spatial grounding from those that capture modality-agnostic noise.

3.2. Visual Anchors and Noise Recurrence

Dual-Anchor Identification via Visualization. Drawing inspiration from recent studies on the internal mechanisms of MLLMs (Zhang et al., 2023; 2024a; Wu & Xie, 2024), which suggest that models inherently possess the capability to identify task-relevant regions despite eventually generating hallucinations, we investigate the evolution of this “internal knowledge” across the layers of the model. By conducting a qualitative evaluation on a diverse set of samples from the COCO dataset (Lin et al., 2014), we identify a dual-anchor mechanism governing the model’s focus during the forward pass. We derive the visual saliency map $\mathbf{M}^{(l, \mathcal{H})}$ for a layer l and a head subset \mathcal{H} by averaging the attention weights from the last query token to the visual token sequence T_{vis} :

$$\mathbf{M}^{(l, \mathcal{H})} = \left[\frac{1}{|\mathcal{H}|} \sum_{h \in \mathcal{H}} \mathbf{A}_h^{(l)}(-1, j) \right]_{j \in T_{vis}} \quad (4)$$

We generate heatmaps for 100 images from the MSCOCO dataset to visualize the attention patterns. As shown in

Figure 2(a), we observe that at intermediate depths, the visually sensitive heads consistently produce **Positive Visual Anchors** that accurately pinpoint task-relevant semantic regions, demonstrating that the model effectively “knows where to look”. Conversely, the initial layers establish **Negative Visual Anchors** characterized by uninformative spatial biases or background noise. While the positive anchors provide grounded visual evidence, this sharp focus is not maintained; as the computation moves toward the final layers, the attention undergoes a structural shift, abandoning these positive anchors and reverting to the negative anchors inherent in the model’s initial layers.

Information Decay and Systematic Noise Recurrence.

To provide a formal basis for the existence and subsequent decay of these visual anchors, we analyze the attention distribution across each layer of the model through multiple metrics and calculate the mean values over the aforementioned 100 images. Specifically, we utilize **Attention Entropy** H to track the stability and dispersion of the visual anchors, calculated as:

$$H(\mathbf{M}^{(l, \mathcal{H})}) = - \sum_{j \in T_{vis}} \mathbf{M}_j^{(l, \mathcal{H})} \log(\mathbf{M}_j^{(l, \mathcal{H})}) \quad (5)$$

Furthermore, to verify the nature of the deep-layer drift, we calculate the **Pearson correlation coefficient** r between the attention maps of the all layers and the Vision distributions (both the positive and negative anchors):

$$r(l) = \frac{\text{Cov}(\mathbf{M}^{(l, \mathcal{H}_{all})}, \mathbf{M}^{(1, \mathcal{H}_{insens})})}{\sigma_{\mathbf{M}^{(l, \mathcal{H}_{all})}} \sigma_{\mathbf{M}^{(1, \mathcal{H}_{insens})}}} \quad (6)$$

The statistical metrics in Figure 2(b) reveal a systematic **Deep-Layer Attention Drift** characterized by the model’s shifting internal focus. While the Attention Entropy exhibits fluctuations across all depths, the intermediate layers function as the peak grounding center where the model establishes Positive Visual Anchors, marked by a combination of low entropy and high semantic alignment. However, this grounded focus significantly diverges as the computation progresses. This drift is evidenced by the divergent trends in Pearson correlation: the correlation with intermediate positive anchors steadily declines in the final stages, while the correlation with early-layer noise priors simultaneously rises. Notably, even in instances where deep layers exhibit lower entropy than the mid-layers, these values often coincide with a high correlation to Layer 1 patterns. This suggests that the model’s late-stage focus is not regaining visual evidence, but is instead being steered toward incorrect regions dictated by linguistic biases. These observations prove that the model’s internal visual evidence is overwritten by a systematic regression toward initial-layer spatial noise. This phenomenon directly motivates our CLVA method, which intervenes in the drifted deep-layer regime by reinforcing

positive anchors and suppressing the recurrence of negative anchors.

4. Methodology

Based on the above findings, we further explore the hallucination mechanism in MLLMs from the perspective of interpretability. Our exploration reveals that the model effectively captures task-relevant regions during intermediate stages, but the subsequent drift in deeper layers represents a systematic regression to early-layer noise priors rather than random dispersion. This suggests that as reasoning depth increases, the model tends to overwrite internal visual evidence with intrinsic spatial biases. To address this, we propose Cross-Layer Visual Anchors (CLVA), a training-free intervention that reinforces grounding knowledge from intermediate layers while actively stripping away recurring noise from the initial layers to restore visual faithfulness. The overview of our method is illustrated in Figure 3.

4.1. Preliminaries

MLLMs typically comprise a visual encoder, a cross-modal interface, and a language decoder (Zhang et al., 2024b; Leng et al., 2024b). During autoregressive inference, the input image is encoded into n visual tokens $T_{vis} = \{v_i\}_{i=1}^n$. These visual tokens are then concentrated to generate the input tokens $[T_{sys}, T_{vis}, T_{txt}]$ for the language decoder, where $T_{sys} = \{t_i\}_{i=0}^{m_b}$ represents the system prompt tokens and $T_{txt} = \{t_i\}_{i=m_b+1}^m$ denotes the instruction tokens. In each self-attention layer of the language decoder, the input hidden states are projected into queries Q , keys K and values V of dimension $(n + m) \times d$. The attention matrix $\mathbf{A} \in \mathbb{R}^{(n+m) \times (n+m)}$ is estimated by:

$$\mathbf{A}_{logits} = \frac{QK^\top}{\sqrt{d}}, \quad \mathbf{A} = \text{softmax}(\mathbf{A}_{logits}) \quad (7)$$

where \mathbf{A}_{logits} is the attention logits before softmax. The matrix \mathbf{A} represents the relevance scores between all token pairs. In the CLVA framework, we specifically intervene in the attention weights directed from the T_{txt} to the T_{vis} . By applying contrastive anchoring to this attention, we steer the model’s focus back to the relevant visual evidence identified in the intermediate layers while suppressing the influence of early-layer spatial priors.

4.2. Dual-Anchor Target and Saliency Masking

To operationalize the attention intervention, we define two contrastive anchors derived from specialized head behaviors. The positive anchor \mathbf{M}_{pos} aggregates attention from vision sensitive heads \mathcal{H}_{sens} at an intermediate layer l_{mid} to capture grounded semantic distributions, while the negative anchor \mathbf{M}_{neg} is extracted from vision-insensitive heads \mathcal{H}_{insens} at the initial layer to characterize inherent spatial

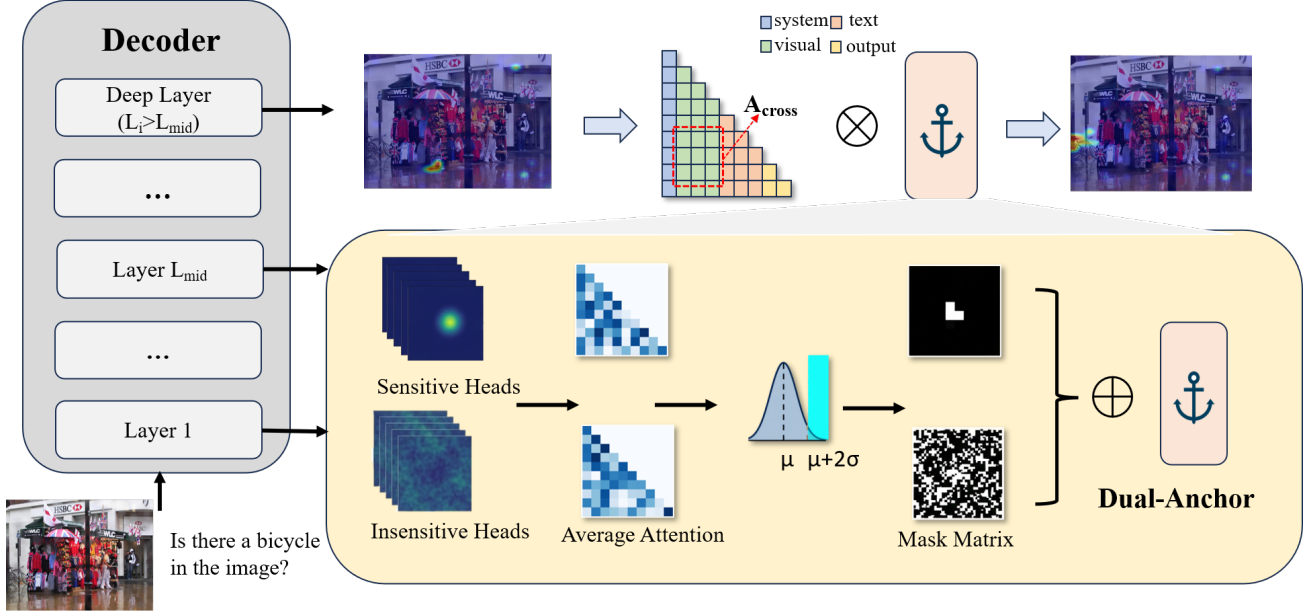


Figure 3. Architecture of CLVA. Based on our attention analysis, we propose a two-step process to anchor drifting attention, where positive anchoring anchors core visual semantic features while negative anchoring excludes background noise using insensitive heads.

biases. For each anchor $k \in \{pos, neg\}$, we employ a statistical outlier detection mechanism to isolate significant regions. Specifically, for each visual token $j \in T_{vis}$, the Z-score $z_j^{(k)}$ is computed as:

$$z_j^{(k)} = \frac{\mathbf{M}_k(j) - \mu_k}{\sigma_k + \epsilon}, \quad j \in T_{vis} \quad (8)$$

where μ_k and σ_k denote the mean and standard deviation of the saliency map \mathbf{M}_k across all visual tokens, and ϵ is a small constant for numerical stability. The resulting binary masks \mathbf{Z}_{pos} and \mathbf{Z}_{neg} are then formulated as the support of spatial outliers exceeding a significance threshold τ :

$$\mathbf{Z}_k(j) = \mathbb{I}(z_j^{(k)} > \tau), \quad j \in T_{vis} \quad (9)$$

In this formulation, \mathbb{I} is the indicator function. These dual masks provide categorical geometric constraints to guide the attention re-anchoring process in the deeper layers.

4.3. Attention Re-anchoring

The intervention process operationalizes the dual-anchor strategy by performing layer-wise rectification within the drift region. Specifically, at each decoding step within the affected layers, the attention matrix \mathbf{A} is adjusted to enhance the model’s focus on relevant visual regions while actively suppressing the erroneous drift toward early-layer noise. For each textual token $i \in T_{txt}$ and visual token $j \in T_{vis}$, the attention weights are modulated by the dual anchors as follows:

$$\tilde{\mathbf{A}}(i, j) = \mathbf{A}(i, j) \cdot (1 + \alpha \mathbf{Z}_{pos}(j) - \beta \mathbf{Z}_{neg}(j)) \quad (10)$$

where α and β are hyperparameters that govern the intensity of positive reinforcement and negative suppression, respectively. To preserve the probabilistic interpretation of the attention mechanism, the modified weights undergo a secondary normalization:

$$\hat{\mathbf{A}}(i, j) = \frac{\tilde{\mathbf{A}}(i, j)}{\sum_j \tilde{\mathbf{A}}(i, j)}, \quad i \in T_{txt} \quad (11)$$

This dual-stage strategy enables the model to dynamically recalibrate its cross-modal alignment without additional training, ensuring that the language decoder remains anchored to high-fidelity visual evidence and effectively mitigating the emergence of hallucinated content in complex reasoning tasks.

4.4. Theoretical Analysis

The re-anchoring of attention weights directly reshapes the output representation O , which serves as the core signal for autoregressive decoding. In the Transformer architecture, the output is computed as $O = AV$, where A is the attention matrix and V the value matrix. By partitioning the sequence into linguistic and visual tokens, this can be decomposed as:

$$O_i = \underbrace{\sum_{j \in T_{sys} \cup T_{txt}} \hat{\mathbf{A}}(i, j) V_j}_{O_P} + \underbrace{\sum_{k \in T_{vis}} \hat{\mathbf{A}}(i, k) V_k}_{O_V} \quad (12)$$

where O_i is the output for query token i . In shallow layers, the visual component O_V typically dominates, reflecting

initial modality fusion. In deeper layers, however, LVLMs naturally exhibit perceptual collapse where $A(i, k)$ for visual tokens T_{vis} diminishes toward zero. Consequently, the linguistic component O_P dominates the output, forcing the hidden state to be updated primarily by language priors stored in the system prompt T_{sys} and preceding context T_{txt} . CLVA intervenes by replacing the original weights with the re-anchored weights \hat{A} . This intervention fundamentally alters the composition of the hidden state through two direct effects:

- **Suppression of Language Priors:** As the mass of \hat{A} for visual tokens increases, the weights for linguistic tokens $T_{sys} \cup T_{txt}$ are proportionally reduced due to the re-normalization. This dampens the magnitude of O_P , thereby mitigating hallucinations driven by excessive reliance on language priors.
- **Visual Signal Purification:** By concentrating the attention mass on regions validated by Z_{pos} and pruning those in Z_{neg} , the visual component O_{vis} is refreshed with high-fidelity semantic evidence.

The intervention framework is compatible with various LVLM paradigms without structural modification. For linear projection, the re-anchoring is applied to the self-attention layers of the decoder. In models utilizing a Q-Former or visual abstractor, the strategy is implemented within the cross-attention mechanism bridging the visual encoder and the LLM.

5. Experiments

5.1. Models and Experimental Setup

Model Selection. We evaluate CLVA on three representative models: LLaVA-1.5(Liu et al., 2024a), Qwen-VL(Bai et al., 2023), and InstructBLIP(Dai et al., 2023). We adopt the 7 billion parameters (7B) version for the language model backbone across all three architectures to ensure a consistent comparison.

Baselines. We compare CLVA against three state-of-the-art training-free methods representing different technical approaches. **IMCCD**(Li et al., 2025a) adopts an improved multimodal contrastive decoding framework to refine output distributions. **MemVR**(Zou et al., 2024) utilizes a visual retracing mechanism to verify generated content against the original visual features. **ClearSight**(Yin et al., 2025) focuses on mitigating hallucinations by amplifying the model’s attention toward image tokens during the decoding process.

Decoding and Hyper-parameters. Greedy search is the default decoding protocol unless otherwise specified. For evaluations involving beam search, the beam size is fixed

at 5. CLVA utilizes the first layer as the negative anchor, while the positive anchor is set to layer $L/2 - 2$, where L denotes the total number of model layers. These specific anchor layers were selected based on preliminary experiments on the MSCOCO validation set to ensure balanced performance. The amplification factor α , the penalty factor β , and the significance threshold τ were set to 14, 0.9, and 2, respectively.

5.2. Hallucination Benchmark Results

CLVA is evaluated on two primary hallucination benchmarks, POPE(Li et al., 2023) and CHAIR(Rohrbach et al., 2018). These datasets assess the model performance from discriminative probing and generative captioning perspectives, respectively.

POPE. This benchmark frames object hallucination as a binary classification task where models must determine the presence of specific objects. The evaluation involves nine distinct subsets constructed from three source datasets: MSCOCO, AOKVQA, and GQA. Each source is paired with three sampling strategies labeled as Random, Popular, and Adversarial. Each subset contains 500 images with 6 questions per image. Following established protocols, a constraint requiring a one-word answer is appended to each query to ensure consistency. Accuracy and F1 score serve as the primary performance metrics.

The results in Table 1 show that CLVA achieves a performance boost compared to other state of the art training free methods. Our approach yields significant improvements in both Accuracy(ranging from 0.59% to 7.13%) and F1 score(ranging from 0.28% to 6.33%). Beyond standard architectures, CLVA also achieves substantial performance enhancements when applied to models utilizing Q former architectures. This demonstrates that our intervention mechanism is not limited to a specific framework but possesses broad applicability across different model designs. While some results for CLVA do not surpass those of IMCCD on the POPE benchmark, our method offers a decisive advantage in terms of computational efficiency. CLVA requires only half the video memory compared to IMCCD and operates at nearly twice the speed during inference. For further details, please refer to Appendix A.

CHAIR. This benchmark provides a systematic framework for evaluating object hallucination in image captioning tasks. Caption accuracy is assessed by comparing mentioned objects against ground truth labels. A hallucination is defined as an object present in the generated description but absent from the ground truth. Following standard experimental protocols, we evaluate on 500 randomly sampled images from the MSCOCO 2014 validation set. The model is prompted to describe the image in detail with a maximum generation length set to 128 tokens. Lower values in these metrics

Table 1. Results on the POPE benchmark. Results are averaged across the MS-COCO, A-OKVQA, and GQA datasets. The best and second best results are bolded and underlined, respectively. “-” indicates the result is not supported by the released implementation.

Evaluation	Methods	Random		Popular		Adversarial		Average	
		F1-score \uparrow	Accuracy \uparrow						
LLaVA-1.5	Greedy	87.18	88.26	84.48	85.02	81.24	81.11	84.30	84.79
	Beam Search	87.26	88.35	84.50	85.03	81.21	81.09	84.32	84.82
	MemVR	87.83	88.40	83.20	84.37	80.61	80.53	83.88	84.43
	ClearSight	88.16	88.77	85.13	85.02	81.44	80.39	84.91	84.72
	IMCCD	<u>88.22</u>	<u>88.82</u>	<u>85.45</u>	<u>86.00</u>	<u>82.07</u>	<u>81.66</u>	<u>85.24</u>	<u>85.49</u>
	CLVA (ours)	88.70	89.37	85.82	86.39	82.50	82.19	85.67	85.98
InstructBLIP	Greedy	81.25	80.75	78.17	76.60	76.12	73.71	78.51	77.02
	Beam Search	81.30	80.80	78.17	76.60	76.09	73.69	78.52	77.03
	MemVR	-	-	-	-	-	-	-	-
	ClearSight	-	-	-	-	-	-	-	-
	IMCCD	<u>85.85</u>	<u>86.30</u>	<u>81.79</u>	<u>81.22</u>	<u>78.90</u>	<u>77.29</u>	<u>82.18</u>	<u>81.60</u>
	CLVA (ours)	87.58	87.88	82.53	81.79	79.47	77.72	83.19	82.46
Qwen-VL	Greedy	84.88	86.34	83.45	84.68	81.93	82.86	83.42	84.62
	Beam Search	84.88	86.24	83.40	85.62	81.97	82.89	83.41	84.91
	MemVR	85.75	87.30	<u>85.19</u>	84.73	82.07	82.90	84.33	84.97
	ClearSight	85.94	87.63	84.83	85.78	81.95	<u>82.94</u>	84.24	85.45
	IMCCD	86.66	87.79	85.50	<u>86.05</u>	82.42	82.84	84.86	86.56
	CLVA (ours)	<u>86.51</u>	<u>87.75</u>	84.74	86.13	<u>82.21</u>	83.45	<u>84.48</u>	<u>85.77</u>

Table 2. CHAIR hallucination evaluation results. The best and second best results are bolded and underlined, respectively.

Methods	LLaVA-1.5			InstructBLIP			Qwen-VL		
	CHAIR _i \downarrow	CHAIR _s \downarrow	Recall \uparrow	CHAIR _i \downarrow	CHAIR _s \downarrow	Recall \uparrow	CHAIR _i \downarrow	CHAIR _s \downarrow	Recall \uparrow
Greedy	53.0	15.2	76.7	57.0	16.7	70.4	6.6	7.0	45.5
Beam Search	55.6	16.0	76.7	56.2	<u>14.7</u>	71.4	6.4	5.7	<u>45.7</u>
MemVR	<u>49.2</u>	<u>12.9</u>	78.4	-	-	-	4.7	4.0	45.3
ClearSight	50.0	13.6	<u>78.8</u>	-	-	-	<u>4.2</u>	<u>3.8</u>	44.0
IMCCD	52.2	13.5	<u>76.6</u>	<u>55.3</u>	17.0	<u>73.0</u>	6.6	5.3	41.7
CLVA (ours)	48.0	12.7	80.2	50.2	14.0	74.0	3.8	2.7	46.3

indicate a higher degree of visual grounding and fewer hallucinations.

The experimental results in Table 2 demonstrate that CLVA yields a significant reduction in hallucination rates across different model architectures. For the LLaVA model, CHAIR_s and CHAIR_i are reduced by 5% and 2.5%, respectively. Similarly, InstructBLIP exhibits even more substantial gains with reductions of 6.8% in CHAIR_s and 2.7% in CHAIR_i. Beyond these primary metrics, all models also show improved performance in Recall, indicating that CLVA successfully reduces hallucinations without sacrificing the descriptive capacity of the models. This performance is particularly evident in long descriptions where attention drift in deep layers typically causes the model to lose focus on visual features. These findings confirm the ability of the method to achieve superior visual grounding and consistency during the auto regressive generation process. The scores achieved by our method highlight the capacity of CLVA to produce descriptions that are both detailed and factually accurate.

5.3. General Benchmark Results

We further evaluate CLVA on general benchmarks to ensure that the suppression of hallucinations does not lead to performance degradation in other core capabilities. We select MME(Fu et al., 2025) as the primary benchmark to assess the balance between perception reliability and general visual understanding.

MME. We report the performance of CLVA on the MME benchmark, which provides a comprehensive assessment of both perception and cognition abilities. To offer a detailed view of the model reliability, we include the total scores for the entire MME collection alongside the individual results for the four specific hallucination subsets. These subsets(existence, count, position, and color) are designed to probe the tendency of the model to generate non existent or incorrect visual details.

We present the results on the MME benchmark in Table 3. We find that all three models show an increase in total scores across the MME hallucination subsets. We observe a

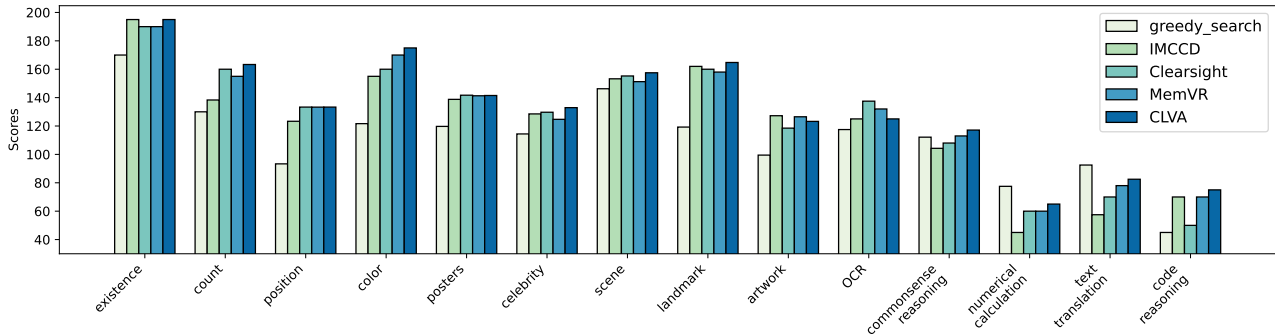


Figure 4. Results of LLaVA-1.5 on MME-Fullset.

Table 3. Results on the hallucination subset of MME. The best performances within each setting are bolded.

Model	Decoding	Object-level		Attribute-level		Total \uparrow
		Existence \uparrow	Count \uparrow	Position \uparrow	Color \uparrow	
LLaVA-1.5	Greedy	170.00	130.00	93.33	121.66	514.99
	Beam Search	170.00	130.00	93.33	121.66	514.99
	MemVR	190.00	155.00	133.33	170.00	648.33
	ClearSight	190.00	160.00	133.33	160.00	643.33
	IMCCD	195.00	138.33	123.33	155.00	611.66
	CLVA (ours)	195.00	163.33	133.33	175.00	666.66
InstructBLIP	Greedy	185.00	60.00	50.00	120.00	415.00
	Beam Search	175.00	68.33	51.66	115.00	409.99
	IMCCD	185.00	55.00	50.00	100.00	390.00
	CLVA (ours)	185.00	55.00	50.00	130.00	420.00
Qwen-VL	Greedy	175.00	140.00	123.33	180.00	618.33
	Beam Search	180.00	141.66	133.33	180.00	634.99
	MemVR	185.00	145.00	123.33	185.00	638.33
	ClearSight	185.00	141.66	148.33	180.00	654.99
	IMCCD	190.00	140.00	138.33	175.00	643.33
	CLVA (ours)	180.00	146.66	158.33	185.00	669.99

particularly significant improvement for LLaVA 1.5, where the score on these subsets rises from 514 to 666. We also evaluate the performance across all 14 subtasks as illustrated in Figure 4. We note that the total MME scores exhibit an upward trend after applying CLVA. Specifically, LLaVA-1.5 shows consistent improvements across all perception capabilities. The performance in numerical calculation and text translation decreases because these tasks primarily involve language decoding rather than visual grounding. These results demonstrate that our method effectively mitigates hallucination phenomena and enhances the overall performance of the models.

5.4. Ablation Studies

Ablation experiments are conducted on the POPE MSCOCO subset and the MME dataset to evaluate the individual contributions of POS and NEG anchors within CLVA. As shown in Table 4, the results demonstrate that both POS and NEG anchors are essential for hallucination mitigation.

The configuration utilizing vision sensitive heads as positive anchors provides the necessary visual grounding to

Table 4. Ablation study of different components in CLVA for LLaVA-1.5. POS and NEG denote positive and negative anchors, while + and - represent the positive and negative usage of anchors, respectively.

POS	NEG	MME (Hallucination)	MME (Overall)	POPE(Random & COCO) F1-score	Accuracy
		514.99	1558.76	84.60	86.76
+		654.66	1843.92	85.39	87.00
	+	643.66	1819.95	85.50	87.06
+	+	666.66	1851.23	86.99	88.26
-	-	505.00	1531.26	83.73	86.20

pull the attention of deep layers back to the correct visual regions. Simultaneously, using insensitive heads as negative anchors successfully suppresses the regressive noise originating from initial layers. The final row of Table 4 represents the negative addition of anchors, where negative anchors from insensitive heads are strengthened while positive anchors from vision sensitive heads are weakened. The significant performance degradation in this setting confirms that the specific orientation of our cross layer mechanism is critical for maintaining visual fidelity. In addition, we conduct further ablation studies on different parameters, with detailed results and analyses provided in the Appendix A.

6. Conclusion

This study investigates the layer wise evolution of visual features and discovers that hallucination in multimodal models is closely linked to deep layer attention drift and the regression toward initial noise from insensitive heads. We propose CLVA, the Cross Layer Visual Anchor method, which is a training-free solution that reinforces critical mid-layer features and pulls drifting attention back to the correct visual regions. Our results across diverse architectures and benchmarks demonstrate that CLVA effectively mitigates hallucination and enhances perception performance without adding significant computational or memory overhead. This work provides a robust and efficient mechanism for improving the visual grounding of vision language systems.

Impact Statement

This paper presents work whose goal is to advance the field of Machine Learning. There are many potential societal consequences of our work, none which we feel must be specifically highlighted here.

References

- Bai, J., Bai, S., Yang, S., Wang, S., Tan, S., Wang, P., Lin, J., Zhou, C., and Zhou, J. Qwen-vl: A frontier large vision-language model with versatile abilities. *arXiv preprint arXiv:2308.12966*, 1(2):3, 2023.
- Bai, Z., Wang, P., Xiao, T., He, T., Han, Z., Zhang, Z., and Shou, M. Z. Hallucination of multimodal large language models: A survey. *arXiv preprint arXiv:2404.18930*, 2024.
- Chen, J., He, J., Shao, Q., Chen, Q., Ying, J., Xu, H., Chen, J., Zheng, J., and Wu, J. Mitigating hallucination of large vision-language models via dynamic logits calibration. *arXiv preprint arXiv:2506.21509*, 2025.
- Chen, K., Zhang, Z., Zeng, W., Zhang, R., Zhu, F., and Zhao, R. Shikra: Unleashing multimodal llm’s referential dialogue magic. *arXiv preprint arXiv:2306.15195*, 2023.
- Chen, Z., Wu, J., Wang, W., Su, W., Chen, G., Xing, S., Zhong, M., Zhang, Q., Zhu, X., Lu, L., et al. Internvl: Scaling up vision foundation models and aligning for generic visual-linguistic tasks. In *Proceedings of the IEEE/CVF conference on computer vision and pattern recognition*, pp. 24185–24198, 2024.
- Cho, Y., Kim, K., Hwang, T., and Cho, S. Do you keep an eye on what i ask? mitigating multimodal hallucination via attention-guided ensemble decoding. *arXiv preprint arXiv:2505.17529*, 2025.
- Dai, W., Li, J., Li, D., Tiong, A., Zhao, J., Wang, W., Li, B., Fung, P. N., and Hoi, S. Instructblip: Towards general-purpose vision-language models with instruction tuning. *Advances in neural information processing systems*, 36: 49250–49267, 2023.
- Devlin, J., Chang, M.-W., Lee, K., and Toutanova, K. Bert: Pre-training of deep bidirectional transformers for language understanding. In *Proceedings of the 2019 conference of the North American chapter of the association for computational linguistics: human language technologies, volume 1 (long and short papers)*, pp. 4171–4186, 2019.
- Fu, C., Chen, P., Shen, Y., Qin, Y., Zhang, M., Lin, X., Yang, J., Zheng, X., Li, K., Sun, X., et al. Mme: A comprehensive evaluation benchmark for multimodal large language models. In *The Thirty-ninth Annual Conference on Neural Information Processing Systems Datasets and Benchmarks Track*, 2025.
- Huang, L., Yu, W., Ma, W., Zhong, W., Feng, Z., Wang, H., Chen, Q., Peng, W., Feng, X., Qin, B., et al. A survey on hallucination in large language models: Principles, taxonomy, challenges, and open questions. *ACM Transactions on Information Systems*, 43(2):1–55, 2025.
- Huang, Q., Dong, X., Zhang, P., Wang, B., He, C., Wang, J., Lin, D., Zhang, W., and Yu, N. Opera: Alleviating hallucination in multi-modal large language models via over-trust penalty and retrospection-allocation. In *Proceedings of the IEEE/CVF Conference on Computer Vision and Pattern Recognition*, pp. 13418–13427, 2024.
- Jiang, Z., Chen, J., Zhu, B., Luo, T., Shen, Y., and Yang, X. Devils in middle layers of large vision-language models: Interpreting, detecting and mitigating object hallucinations via attention lens. In *Proceedings of the Computer Vision and Pattern Recognition Conference*, pp. 25004–25014, 2025.
- Leng, S., Zhang, H., Chen, G., Li, X., Lu, S., Miao, C., and Bing, L. Mitigating object hallucinations in large vision-language models through visual contrastive decoding. In *Proceedings of the IEEE/CVF Conference on Computer Vision and Pattern Recognition*, pp. 13872–13882, 2024a.
- Leng, S., Zhang, H., Chen, G., Li, X., Lu, S., Miao, C., and Bing, L. Mitigating object hallucinations in large vision-language models through visual contrastive decoding. In *Proceedings of the IEEE/CVF Conference on Computer Vision and Pattern Recognition*, pp. 13872–13882, 2024b.
- Li, J., Li, D., Xiong, C., and Hoi, S. Blip: Bootstrapping language-image pre-training for unified vision-language understanding and generation. In *International conference on machine learning*, pp. 12888–12900. PMLR, 2022.
- Li, J., Zhang, J., Jie, Z., Ma, L., and Li, G. Mitigating hallucination for large vision language model by inter-modality correlation calibration decoding. *arXiv preprint arXiv:2501.01926*, 2025a.
- Li, Y., Du, Y., Zhou, K., Wang, J., Zhao, W. X., and Wen, J.-R. Evaluating object hallucination in large vision-language models. In *Proceedings of the 2023 Conference on Empirical Methods in Natural Language Processing*, pp. 292–305, 2023.
- Li, Y., Wang, H., Ding, X., Wang, H., and Li, X. Token activation map to visually explain multimodal llms. *arXiv preprint arXiv:2506.23270*, 2025b.

- Li, Z., Shi, H., Gao, Y., Liu, D., Wang, Z., Chen, Y., Liu, T., Zhao, L., Wang, H., and Metaxas, D. N. The hidden life of tokens: Reducing hallucination of large vision-language models via visual information steering. *arXiv preprint arXiv:2502.03628*, 2025c.
- Lin, T.-Y., Maire, M., Belongie, S., Hays, J., Perona, P., Ramanan, D., Dollár, P., and Zitnick, C. L. Microsoft coco: Common objects in context. In *European conference on computer vision*, pp. 740–755. Springer, 2014.
- Liu, H., Li, C., Li, Y., and Lee, Y. J. Improved baselines with visual instruction tuning. In *Proceedings of the IEEE/CVF conference on computer vision and pattern recognition*, pp. 26296–26306, 2024a.
- Liu, H., Li, C., Li, Y., Li, B., Zhang, Y., Shen, S., and Lee, Y. J. Llanext: Improved reasoning, ocr, and world knowledge, 2024b.
- Park, Y., Lee, D., Choe, J., and Chang, B. Convis: Contrastive decoding with hallucination visualization for mitigating hallucinations in multimodal large language models. In *Proceedings of the AAAI Conference on Artificial Intelligence*, volume 39, pp. 6434–6442, 2025.
- Rohrbach, A., Hendricks, L. A., Burns, K., Darrell, T., and Saenko, K. Object hallucination in image captioning. In *Proceedings of the 2018 Conference on Empirical Methods in Natural Language Processing*, pp. 4035–4045, 2018.
- Tang, L., Zhuang, X., Yang, B., Hu, Z., Li, H., Ma, L., Ru, J., and Zou, Y. Not all tokens and heads are equally important: Dual-level attention intervention for hallucination mitigation. *arXiv preprint arXiv:2506.12609*, 2025.
- Wadkar, S. N., Chaurasia, A., Chadha, A., and Culurciello, E. The evolution of multimodal model architectures. *arXiv preprint arXiv:2405.17927*, 2024.
- Wan, Z., Zhang, C., Yong, S., Ma, M. Q., Stepputtis, S., Morency, L.-P., Ramanan, D., Sycara, K., and Xie, Y. Only: One-layer intervention sufficiently mitigates hallucinations in large vision-language models. *arXiv preprint arXiv:2507.00898*, 2025.
- Wang, C., Chen, X., Zhang, N., Tian, B., Xu, H., Deng, S., and Chen, H. Mllm can see? dynamic correction decoding for hallucination mitigation. *arXiv preprint arXiv:2410.11779*, 2024a.
- Wang, W., Lv, Q., Yu, W., Hong, W., Qi, J., Wang, Y., Ji, J., Yang, Z., Zhao, L., XiXuan, S., et al. Cogvlm: Visual expert for pretrained language models. *Advances in Neural Information Processing Systems*, 37:121475–121499, 2024b.
- Wang, X., Pan, J., Ding, L., and Biemann, C. Mitigating hallucinations in large vision-language models with instruction contrastive decoding. In *Findings of the Association for Computational Linguistics ACL 2024*, pp. 15840–15853, 2024c.
- Wang, Y., Bi, J., Pirk, S., Ma, Y., et al. AscD: Attention-steerable contrastive decoding for reducing hallucination in mllm. *arXiv preprint arXiv:2506.14766*, 2025.
- Wu, P. and Xie, S. V?: Guided visual search as a core mechanism in multimodal llms. In *Proceedings of the IEEE/CVF Conference on Computer Vision and Pattern Recognition*, pp. 13084–13094, 2024.
- Yang, C., Yuan, J., Cai, S., Jiang, J., and Hu, C. Heaven-sent or hell-bent? benchmarking the intelligence and defectiveness of llm hallucinations. *arXiv preprint arXiv:2512.21635*, 2025.
- Yin, H., Si, G., and Wang, Z. ClearSight: Visual signal enhancement for object hallucination mitigation in multimodal large language models. In *Proceedings of the Computer Vision and Pattern Recognition Conference*, pp. 14625–14634, 2025.
- Yu, T., Zhang, H., Li, Q., Xu, Q., Yao, Y., Chen, D., Lu, X., Cui, G., Dang, Y., He, T., et al. Rlaif-v: Open-source ai feedback leads to super gpt-4v trustworthiness. In *Proceedings of the Computer Vision and Pattern Recognition Conference*, pp. 19985–19995, 2025.
- Zhang, J., Khayatkhoei, M., Chhikara, P., and Ilievski, F. Visual cropping improves zero-shot question answering of multimodal large language models. In *RO-FoMo: Robustness of Few-shot and Zero-shot Learning in Large Foundation Models*, 2023.
- Zhang, J., Hu, J., Khayatkhoei, M., Ilievski, F., and Sun, M. Exploring perceptual limitation of multimodal large language models. *arXiv preprint arXiv:2402.07384*, 2024a.
- Zhang, J., Khayatkhoei, M., Chhikara, P., and Ilievski, F. Mllms know where to look: Training-free perception of small visual details with multimodal llms. In *The Thirteenth International Conference on Learning Representations*, 2025.
- Zhang, Y.-F., Yu, W., Wen, Q., Wang, X., Zhang, Z., Wang, L., Jin, R., and Tan, T. Debiasing multimodal large language models. *arXiv preprint arXiv:2403.05262*, 2024b.
- Zhu, D., Chen, J., Shen, X., Li, X., and Elhoseiny, M. Minigt-4: Enhancing vision-language understanding with advanced large language models. In *The Twelfth International Conference on Learning Representations*, 2024.

Zhu, L., Chen, T., Xu, Q., Liu, X., Ji, D., Wu, H., Soh, D. W., and Liu, J. Popen: Preference-based optimization and ensemble for lvlm-based reasoning segmentation. In *Proceedings of the Computer Vision and Pattern Recognition Conference*, pp. 30231–30240, 2025.

Zou, X., Wang, Y., Yan, Y., Lyu, Y., Zheng, K., Huang, S., Chen, J., Jiang, P., Liu, J., Tang, C., et al. Look twice before you answer: Memory-space visual retracing for hallucination mitigation in multimodal large language models. *arXiv preprint arXiv:2410.03577*, 2024.

A. Additional Experimental Results

A.1. Speed and Memory Comparison

We conduct our experiments on a single NVIDIA H20 GPU. We compare the resource consumption of our proposed CLVA and IMCCD on the POPE dataset, as shown in Table 5. We find that CLVA introduces only minimal additional overhead compared to the original baseline model, which demonstrates the clear advantage of our method in terms of resource consumption. Therefore, although some of our experimental results do not exceed those of IMCCD, our advantages in terms of inference speed and memory efficiency remain very large. When the difference is the greatest, the memory we require is only half of that needed for IMCCD, while our speed is about twice as fast.

Table 5. Comparison of inference speed and GPU memory usage for different models and methods on the POPE dataset

Model	Method	Accuracy	Total Time	GPU-Memory	Latency/Example
LLaVA-1.5	Greedy	84.79	0:7:48	15.7G	0.155s
	IMCCD	85.49	0:16:38	18.7G	0.353s
	CLVA (ours)	85.98	0:7:54	15.8G	0.157s
InstructBLIP	Greedy	77.02	0:5:07	16.6G	0.102s
	IMCCD	81.60	0:10:30	16.7G	0.207s
	CLVA (ours)	82.46	0:5:22	16.6G	0.105s
Qwen-VL	Greedy	84.62	0:14:34	20.4G	0.296s
	IMCCD	86.56	0:35:22	24.9G	0.709s
	CLVA (ours)	86.77	0:15:45	20.4G	0.321s

A.2. Ablation Study

We conduct parameter sensitivity experiments for α and β on the POPE random coco subset, as shown in Figure 5. We observe that when the positive anchor modification parameter α exceeds 14, the model performance begins to decline. Similarly, the performance of the model decreases as the negative anchor correction parameter β provides less suppression. We believe the performance drop associated with an excessively large α occurs because the model focuses too intensely on visual regions, which eventually disrupts the original understanding of the overall semantics. This demonstrates that while anchoring is effective, maintaining a balance between visual focus and linguistic context is crucial for maintaining the robustness of the autoregressive generation process.

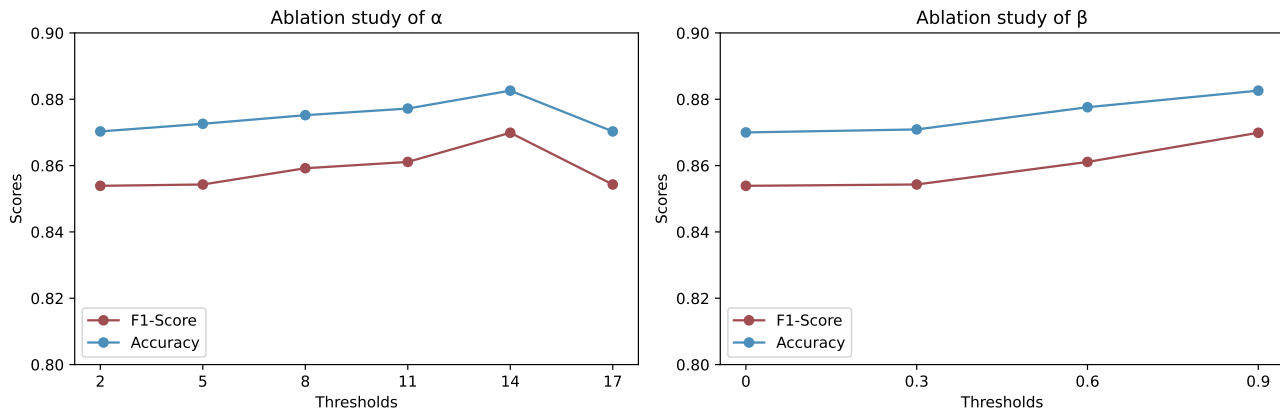


Figure 5. Ablation study of α and β

A.3. Experimental Results with Nucleus Sampling

We document the performance of CLVA during nucleus sampling on the coco subset of POPE. As shown in Table 6, we include these findings in the appendix to provide a more comprehensive view, as stochastic decoding typically lacks the high

reproducibility associated with greedy search. Our evaluation spans three separate models to ensure the broad applicability of our findings. We observe that CLVA consistently maintains a clear performance margin over all baseline methods under these sampling conditions. This sustained advantage is a direct result of the double anchors mechanism.

Table 6. Results of different models using nucleus sampling on the POPE dataset

	Method	LLaVA-1.5		InstructBLIP		Qwen-VL	
		F1	Accuracy	F1	Accuracy	F1	Accuracy
random	sample	81.94	83.76	81.12	81.50	83.72	85.73
	ours	82.97	84.33	84.06	84.43	84.87	86.56
popular	sample	80.86	82.56	78.74	78.50	83.03	84.96
	ours	83.52	84.96	82.54	81.55	83.54	85.86
adversarial	sample	78.43	79.73	77.91	77.43	81.43	83.13
	ours	79.83	80.76	80.78	80.30	83.04	84.53

A.4. Visualization of Attention Heatmaps

We provide visualizations of the attention heatmaps from the subsequent layers of the CLVA-weighted model to demonstrate the effectiveness of our weighting mechanism. We observe that the significant attention drift typically found in deeper layers is successfully corrected through the application of CLVA. As illustrated in Figure 7 and Figure 6, our method pulls the drifted attention back to the precise visual regions that were previously ignored or misaligned. We achieve this spatial recalibration through the double anchors mechanism, which redirects the focus of the model toward relevant image features. By leveraging the visual guidance and suppressing the noise from insensitive heads, we ensure that the model maintains a strong and accurate visual grounding during the autoregressive generation process.

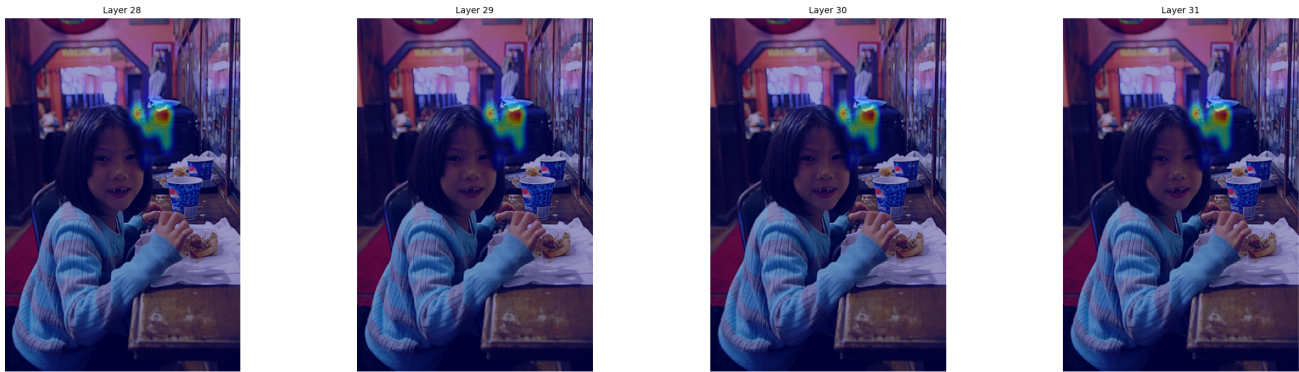


Figure 6. Is there a backpack in the image?



Figure 7. Is there a bicycle in the image?

A.5. Case study on LLaVA-Bench

We evaluate CLVA on the LLaVA-Bench dataset using the LLaVA-1.5 model to assess its performance in more complex and open ended scenarios. As shown in (Figure 8, Figure 9, Figure 10). LLaVA Bench is designed to test the capabilities of models in real world settings, focusing on detailed descriptions, complex reasoning, and conversational logic. We compare our results with the original baseline model to demonstrate the practical benefits of the double anchors mechanism. We find that CLVA consistently produces more accurate and grounded responses than the baseline. This improvement is particularly evident in long generation tasks where the model must maintain a consistent focus on specific image regions. By utilizing insensitive heads to mitigate the impact of linguistic priors, we show that our training-free method effectively prevents the model from generating hallucinations during the autoregressive process, leading to a higher degree of alignment between the visual input and the generated text.

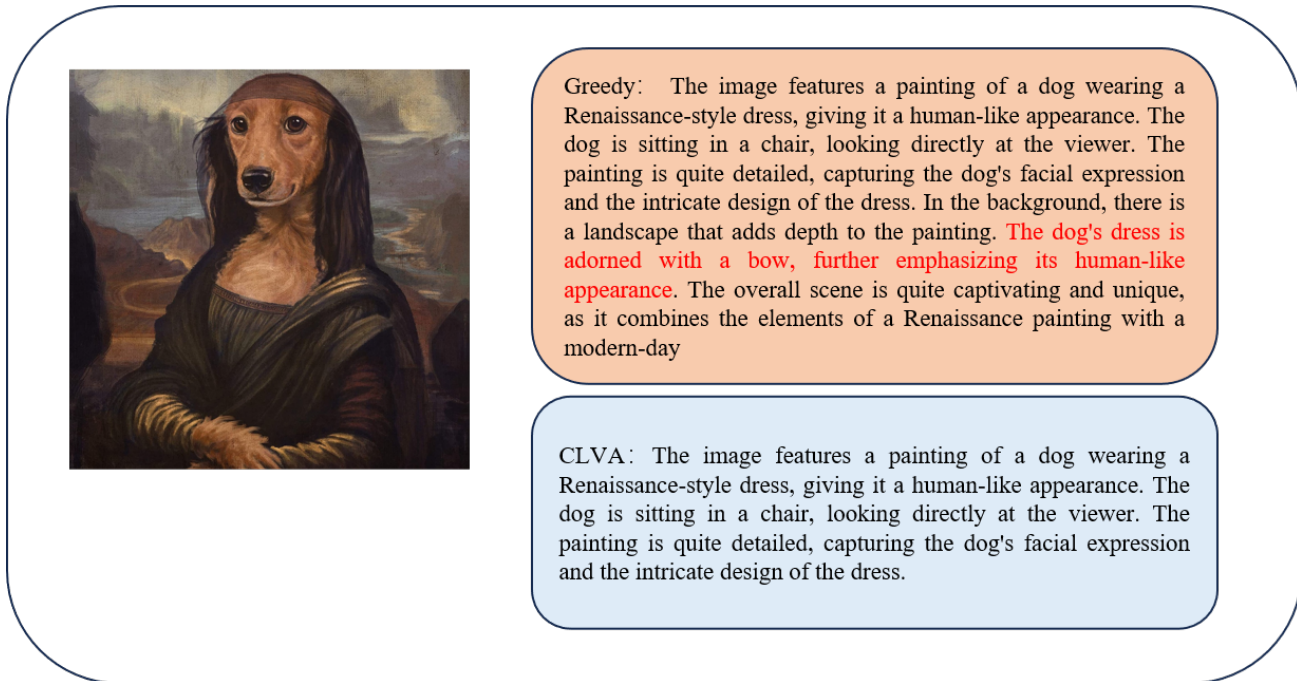


Figure 8. An example of the LLaVA-1.5 model on LLaVA-Bench; red text indicates incorrect answers.

B. Theoretical Analysis

B.1. Analysis of Q-former Architectures

We investigate the theoretical limitations of applying attention modifications directly to the compressed output of a Q-former. In architectures like BLIP-2, the Q-former compresses a large set of raw visual features into a significantly smaller set of latent tokens Z . When the LLM performs cross-attention over these tokens, the spatial information is already highly diffused. We find that applying the double anchors mechanism at the LLM decoder level for these compressed tokens leads to suboptimal results. The core of our modification follows the weighting formula:

$$\tilde{\mathbf{A}}(i, j) = \mathbf{A}(i, j) \cdot (1 + \alpha \mathbf{Z}_{pos}(j) - \beta \mathbf{Z}_{neg}(j)) \quad (13)$$

where $\mathbf{A}(i, j)$ represents the original attention weight, and \mathbf{Z}_{pos} and \mathbf{Z}_{neg} are the positive visual anchors and negative noise anchors derived from insensitive heads. The primary theoretical challenge is that each compressed token z_j no longer maintains a one to one correspondence with a specific spatial region (x, y) in the original image. Instead, each token is a high-level semantic aggregator. If we were to apply the above formula to the LLM attention weights $\mathbf{A}(i, j)$ targeting these compressed tokens, the amplification or suppression would act on a "blurred" semantic representation. This leads to a loss of spatial precision and disrupts the delicate balance of the latent space, which we can characterize as a reduction in the mutual information between the original image and the weighted tokens. To overcome this, we adapt the double



Greedy: The image features a close-up of three Nintendo cups, each depicting the beloved character, Mario. The cups are arranged close together, showcasing their unique appearance. The middle cup hosts the largest of the three and is positioned closest to the center of the image. **Additionally, there is a coffee cup located slightly to the left of the series of cups.**

CLVA: The image features a collection of cups with Mario characters printed on them, arranged on a shelf. There are three cups in total, each with a Mario character on them. The cups are likely part of a collection or a display, showcasing the popularity of the Mario character.

Figure 9. An example of the InstructBLIP model on LLaVA-Bench; red text indicates incorrect answers.

anchors mechanism by applying the weighting formula directly within the internal cross-attention layers of the Qformer itself. During the compression phase, the Qformer queries Q interact with the raw image features K, V . By applying the modification:

$$\tilde{\mathbf{A}}_{Qf}(i, j) = \mathbf{A}_{Qf}(i, j) \cdot (1 + \alpha \mathbf{Z}_{pos}(j) - \beta \mathbf{Z}_{neg}(j)) \quad (14)$$

We ensure that the latent queries are forced to aggregate information from the relevant visual regions while actively suppressing background or linguistic noise before the compression is finalized. This internal application of double anchors ensures that the resulting compressed tokens provided to the LLM are spatially "cleaner" and semantically richer. Our experiments confirm that this architectural adaptation leads to a significant performance boost, as it mitigates the attention drift at the source of the visual representation rather than attempting to correct it after the spatial information has already been compressed.

B.2. Motivation for Distinguishing Attention Heads

We analyze the necessity of separating attention heads into functional categories rather than applying a global average for anchor extraction. Our theoretical framework relies on the observation that attention heads in Large Multi Modal Models exhibit high degrees of functional specialization. Specifically, vision sensitive heads focus on grounded object features, while insensitive heads primarily process linguistic transitions or global background noise. We argue that a simple averaging of all heads $\mathbf{Z}_{avg} = \frac{1}{H} \sum_{h=1}^H \mathbf{Z}_h$ acts as a low pass filter that blurs these distinct signals. If we were to replace our specific anchors with a global average in the weighting formula:

$$\tilde{\mathbf{A}}(i, j) = \mathbf{A}(i, j) \cdot (1 + (\alpha - \beta) \mathbf{Z}_{avg}(j)) \quad (15)$$

the contrastive power of the mechanism is lost. In this scenario, the positive signal from sensitive heads is diluted by the noise from insensitive heads, while the negative anchor \mathbf{Z}_{neg} becomes "contaminated" with actual visual information. This leads to a significant reduction in the signal to noise ratio of the visual guidance.

By isolating insensitive heads, we obtain a "pure" baseline that represents the internal linguistic bias of the model. This allows the negative anchor \mathbf{Z}_{neg} to precisely identify which regions are being attended to due to auto-regressive language patterns rather than actual visual evidence. Simultaneously, extracting \mathbf{Z}_{pos} from sensitive heads ensures that the positive reinforcement is concentrated on high value visual features.

We conclude that this distinction is critical for the success of the double anchors mechanism. It creates a contrastive effect that allows our weighting formula to effectively "push" the attention of the model away from linguistic hallucinations and "pull" it toward grounded visual tokens. Without this separation, the model would fail to distinguish between meaningful

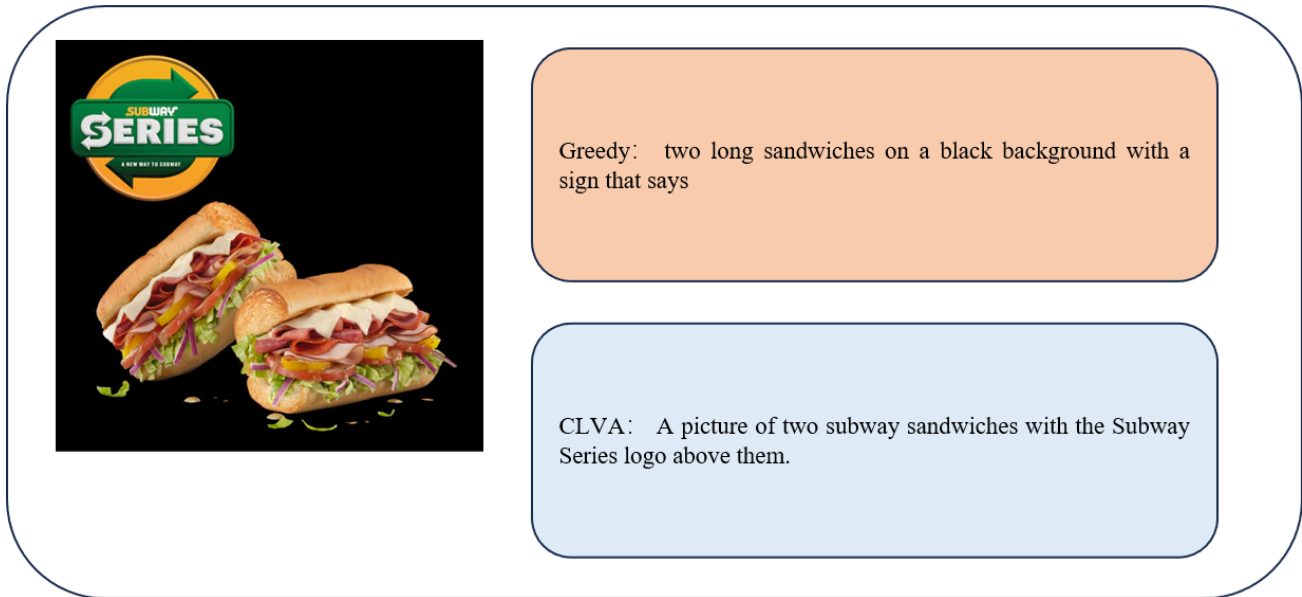


Figure 10. An example of the Qwen-VL model on LLaVA-Bench; red text indicates incorrect answers.

visual cues and the inherent noise of the deep layers, ultimately leading to the very attention drift that CLVA is designed to prevent.